Energy-Based Strength Theory for Soft Elastic Membranes

Reza Pourmodheji
Department of Mechanical Engineering,
The City College of New York,
New York, NY 10031
e-mail: rpourmodheji@ccny.cuny.edu

Shaoxing Qu
Department of Engineering Mechanics,
State Key Laboratory of Fluid Power and Mechatronic Systems,
Key Laboratory of Soft Machines and Smart Devices of Zhejiang Province,
Zhejiang University,
Hangzhou 310027, China
e-mail: squ@zju.edu.cn

Honghui Yu[1]
Department of Mechanical Engineering,
The City College of New York,
New York, NY 10031
e-mail: yu@ccny.cuny.edu

In the previous studies by the authors and others, it was demonstrated that there are two possible defect growth modes and a characteristic material length for any soft material. For a pre-existing defect smaller than the material characteristic length, the energy is dissipated all around the defect as it grows and the critical load for the growth is independent of the defect size. For defects larger than the characteristic length, the growth is by cracking and the energy is dissipated along a plane. Thus, the critical load for the growth is size dependent and can be predicted by fracture mechanics. In this study, we apply the same energy-based argument to the failure of thin membranes, with the focus on the first growth mode that gives the maximum critical load. We assume that strain localization due to damage is the precursor to rupture, and hence, we model the corresponding zone as a through-thickness hole, with its size smaller than the material characteristic length. The defect grows when the elastic energy relaxed by the growth is enough to provide the energy needed for internal microstructure changes. This leads us to the size-independent failure conditions for membranes under the biaxial load. The conditions are expressed in terms of either two principal stretches or two principal stresses for two different types of materials. For verification, we test the theory using the published experimental data on natural and styrene-butadiene rubber. By using the experimental data from equal biaxial loading, we predict the critical principal stretch ratios and critical stresses for different biaxialities. The predictions agree well with the experimental results.
[DOI: 10.1115/1.4043145]

1 Introduction

Throughout the literature, it has been postulated that the common source of failure in soft elastic materials is the growth of microscopic defects [1–13]. The defects can be inhomogeneities such as microcavities, microcracks, and weakened or highly strained zones. Therefore, studying the defect growth criteria has been of great interest. However, the main goal of such studies is to predict the failure, which is mainly signaled through a critical state of stress or deformation.

The first approach in studying the mechanical failure gives various classical strength theories [14–16]. These theories usually do not make assumptions on microstructure of the materials and give the size-independent critical load.

However, for soft materials, there is still no widely accepted strength theory. For a neo-Hookean material as an early model for rubbers, an ultimate hydrostatic tensile load of $p_u = 5E/6$ was proposed by Gent and Lindley [1]. Their ultilmate load was obtained by taking the limit of the elastic solution as the cavity elastically expands to infinity. However, the theory did not address the material failure itself, and such elastic limit load does not exist for many other polymers [11,17–20].

Another challenge in strength theory approaches is that although the critical load can be measured for a specific loading type, such as uniaxial loading, it is not easy to be extended to the general multiaxial loading cases. This is especially the case for highly nonlinear elastomers. Some other examples of strength theories are based on ultimate stretch ratios or ultimate stretch tensor invariants such as I_1. However, they are not so satisfactory for general multi-axial loadings [21]. The idea that cavitation or failure is not only determined by deformation has been transcribed in the literature and thoroughly reviewed recently by Poulain et al. [13].

The second type of approach in studying failure leads to the development of fracture mechanics, which gives the size-dependent critical stress. Fracture mechanics introduces an important material property: fracture toughness. Given a pre-cut large crack with a certain size, fracture toughness can be measured experimentally. The critical load for crack propagation is then determined by matching the energy-release rate or J-integral to the fracture toughness [11,22–33]. However, applying the fracture criterion to a real material needs the initial crack size. That is usually not available in practical applications, especially in design processes and in small scale structures.

Continuum damage theory or phase-field models [34–45] might be one way of resolution in defect initiation. For example, energy limiter [39], local ultimate state variables [46], and a damage variable [44] are chosen as failure measures. However, in some cases, the related parameters are hard or impossible to be calibrated by experiments because the evolution in this incubation or incipient stage may not be shown explicitly or externally.

In a recent study by the authors [47,48], we proposed two defect growth modes, omnidirectional growth, and cracking. In the first mode, energy is dissipated all around the defect, and in the second mode, energy is only dissipated in a layer next to the cracking plane. The theory suggests that there is a characteristic length for any soft material. If the defect is smaller than the characteristic length, the defect grows by omnidirectional expansion, and the critical load is size-insensible, as in the strength theories. If the defect is greater than the characteristic length, the defect grows by cracking and size-dependent fracture mechanics theories are applied. The argument is mainly from the geometric consideration and thermodynamics. The idea of the two-stage growth was also discussed in a series of papers recently, including a physics-based theory in forms of material chain scission [49] and progressive damage models [44,50]. The models used the phase-field–based approach, so that the two growth modes were inherently embedded in: for the small flaw size, the growth is volumetric, and for the large flaw size, the growth is by cracking.

The second mode has been studied extensively in fracture mechanics. When Irwin [51] proposed his fracture criterion for steel, he assumed a self-similar growing crack: as the crack

[1]Corresponding author.

Contributed by the Applied Mechanics Division of ASME for publication in the Journal of Applied Mechanics. Manuscript received December 4, 2018; final manuscript received March 6, 2019; published online April 19, 2019. Assoc. Editor: Pedro Reis.

propagates, it leaves behind a band of constant thickness that experiences plastic loading and unloading. This means that energy dissipation, as the dominant contributor to the fracture toughness, is proportional to the new surface area created by cracking. This scenario is schematically depicted in Fig. 1(*a*). However, when a crack is very small, especially when it is smaller than the band thickness, the assessment should be reexamined. Because in such cases, the dissipation band of constant thickness has not been established yet. This is schematically depicted in Fig. 1(*b*). In Refs. [47,48], we considered the simple case of a solid under hydrostatic tension p at the remote. Due to the large compliance of the elastomer materials, the defect was modeled as a spherical cavity of radius A. No matter which growth mode, the reduction of mechanical energy associated with the defect growth can always be written in the form of

$$-d\Pi = [4\pi CA^2 dA]\bar{\mathcal{G}}\left(\frac{p}{C}\right) \tag{1}$$

where Π is the mechanical energy including strain energy, and the potential of external forces. $\bar{\mathcal{G}}$ is a dimensionless function of the remote stress p and C, which is the initial elastic property, $C = E/6$. E is initial Young's modulus. For the cracking mode, the energy needed in creating new surface is $2\pi A\Gamma_s dA$, where Γ_s is the fracture toughness. Equating this energy to the reduction of mechanical energy in Eq. (1) gives the familiar size-dependent critical stress for crack growth,

$$\frac{p_{cr}}{C} = \bar{\mathcal{G}}^{-1}\left(\frac{\Gamma_s}{2CA}\right) \tag{2}$$

However, in the first growth mode, since the energy dissipation is all around the defect, the energy needed for irreversible growth of cavity is $4\pi A^2\Gamma_p\, dA$, where Γ_p is the volume processing energy, which is the energy needed to permanently move one unit of material volume next to the hole away from its original location. The possible mechanism for the nonelastic deformation could be breaking bonds, untangling chains, and chain sliding. Equating the energy barrier for the growth with the relaxed mechanical energy in Eq. (1) gives the size-independent critical load for the growth:

$$\frac{p_{cr}}{C} = \bar{\mathcal{G}}^{-1}\left(\frac{\Gamma_p}{C}\right) \tag{3}$$

When the defect is very small, we proved in Ref. [48] that the omnidirectional growth mode is predominant. As the defect grows to a characteristic size of A^*, scaled with the ratio Γ_s/Γ_p, the growth mode transits from the first mode to the cracking mode. For $A > A^*$, the defect grows by cracking, which is well discussed in fracture mechanics.

The flaw insensibility in small scales was first studied by Gao et al. [52] as a lesson from nature, where they demonstrated that biological materials select certain structural features in a nanoscale to optimize their strength. The concept of flaw size dependence was revisited by Chen et al. [53] when studying fatigue. They proposed somewhat same characteristic length when discussing the notch sensitivity. They estimated the typical values of A^* to be of ~1 mm for natural rubber (NR) and ~10 mm for tough hydrogels [53]. Mao et al. [49] then gave a clear physical picture using an elastomer chain model and showed that the fracture stretch loses the dependency on the small notch size. Volokh [54] also estimated a length scale for natural rubber using the work done to failure in their energy limiter theory and the fracture toughness estimated by Rivlin and Thomes [23]. The critical load is insensitive to the defect size if it is smaller than the transitional defect size.

In the above discussion, we assume that the energy barrier for the defect growth is mainly due to the energy dissipation around the defect. Recently, Poulain et al. [55] and Kumar et al. [45] postulated and experimentally showed that cavitation is not purely dissipative, i.e., defects in deca-microns can be healed and disappear on unloading, leaving an intact material zone. Thus, besides dissipative energy, the energy reduction in healing process is also a part of the energy barrier. One part of this healing energy is surface energy. As in metal or ceramics, it is proportional to the increment of surface area. In soft materials, however, the kinetic processes involved in healing, such as recombinations, recoils and mass transport, all occur in the zone around the defect with a finite volume. Thus, we define Γ_p as the total energy needed to drive the unit volume of mass out of its original location next to the cavity surface. It includes the dissipative energy and the volumetric part of the healing energy.

It is novel to see that a size-independent failure criterion similar to classic strength theories can be derived from the Griffith [22] energy criterion, which is inherently size-dependent. This paper applies the proposed energy-based idea to the failure of thin membrane and derives the explicit failure conditions in terms of remote stresses or stretches. Nait-Abdelaziz et al. [29] studied the membrane failure under general biaxial loading by assuming an initial defect size and applying fracture mechanics criterion. The fundamental differences between the current study and their approach is that we do not need a specific defect size as they estimated certain sizes. We adopt a different defect growth criterion, and

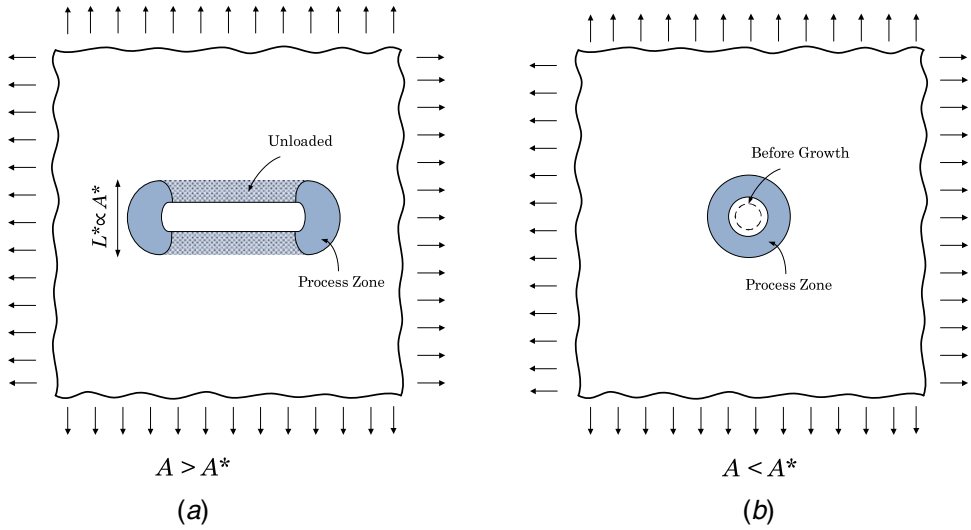

Fig. 1 Two modes of defect growth: (*a*) cracking by dissipating energy along a layer of finite thickness and (*b*) omnidirectional growth by dissipating energy all around the defect

the results are independent of defect size as long as it is smaller than the characteristic size.

The failure of thin soft membrane has been of a great interest in recent years. For example, the natural cavitation and failure in thin membranes of biological tissues and hydrogels [56–60] and dielectric elastomers [61–65] fit into this study. For many soft membranes in practical application, we believe that there is no initial crack or defect that is larger than the characteristic material length. Thus, the critical load for the first growth mode might be more practically relevant than that of the cracking mode, and a size-independent failure criterion might be more useful in the design process.

The objective of this paper is to derive practical and directly usable failure criteria in terms of principal stretches or principal stresses for a membrane under general biaxial loading. Two classes of materials will be examined, one is called I_1-materials, whose strain energy density functions mainly depend on the first invariant of Right Cauchy-Green deformation tensor, and the second is called I_1-I_2-materials, whose energy density functions depend on both invariants, I_1 and I_2.

In Sec. 2, the first growth mode will be considered for the failure of thin membranes. In the first part of the section, the configurational driving force for the defect growth will be calculated as a function of applied load for equi-biaxial loading. We propose to use the driving force in equi-biaxial case to match the experimental results to get a key parameter in the model, the volume process energy Γ_p. In the second part of the section, we calculate the driving forces for the general biaxial-loading cases. By using the obtained Γ_p from equi-biaxial and the driving force of general biaxial loading, we are able to obtain the failure conditions in terms of remote loading, either two principal stretches or two principal stresses. To verify the reliability of the proposed approach, we compare the predictions with the experimental results obtained by Hamdi et al. [66].

2 Thin Membranes Under Biaxial Stretching

Consider a thin membrane under general in-plane biaxial loading. We assume that rupture of membrane is first triggered by strain localization, internal microstructural change, and energy dissipation at certain zone, as shown schematically by the shaded area in Fig. 2(*a*). Physically, it could be due to preexisting defects such as surface defects, inhomogeneities, or the so-called damage zone as described in damage mechanics or phase-field models. As the external load increases, the zone evolves and grows irreversibly. However, it is surrounded by the elastic zone outside. Any bond breaking, chain untangling and sliding in the damaged zone cause strain relaxation in the surrounding elastic zone. Mathematically, for the elastic field of the surrounding zone, which has a relatively large size, the damage zone can be replaced by or modeled as a through-thickness hole of certain size A, as shown in Fig. 2(*b*). The model is valid as long as the displacements along the dashed lines are same as shown in Figs. 2(*a*) and 2(*b*). We assume that the hole is smaller than the material characteristic length A^*, in consistence with the first growth mode, which is usually the case of failure initiation in soft materials. Since the critical load for the first growth mode is size independent, the defect size is not needed to calculate the critical load.

Assume that the thin membrane depicted in Fig. 2 is made of an incompressible isotropic hyperelastic material with initial thickness T and side length $2B$. It is under remote biaxial Cauchy stresses p_1 and p_2. The two corresponding principal stretches are λ and λ^n. n is the ratio of two principal strains and represents the load biaxiality; for example, $n=1$ is for equi-biaxial loading and $n=0$ for pure shear (second direction constrained). In the thickness direction, the third principal stress is $p_3 \approx 0$, and the third principal stretch is $\lambda^{-(n+1)}$ due to incompressibility.

We assume that the hole is circular with the undeformed radius A and in the middle of the sheet. The circular shape is chosen so that only one geometric parameter is needed to describe the configuration of the defect, and also we intend to remove any directional preference other than the external loading itself. Moreover, if there is a real through-thickness and irregular-shaped defect in the membrane, owing to its high stretchability, the stress localization around the defect would soon smooth out as the remote load increases. In fact, the field slightly away from the defect is insensitive to the original shape of the defect. Thus, as a first-order approximation, a strain localized damage zone or physically real through-thickness defect of any irregular shape could be treated as a circular hole.

2.1 Equi-Biaxial Loading. Equi-biaxial loading is easier to carry out experimentally, so we choose it to determine the volume processing energy Γ_p from the critical stretch ratio. For mathematical convenience, now we assume the external boundary is a circle of radius B so that we could use polar coordinates. For this axisymmetric problem, we can get the stress and deformation fields by solving an ordinary differential equation (ODE). The equi-biaxial solution also will be used as a benchmark to validate the finite element solution in Sec. 2.2.

As the external load is applied, the radius of the hole stretches to a and the outer boundary to b. The current geometry of the deformed body is described by the function $r(R)$, where R and r are the radial coordinates before and after deformation, respectively.

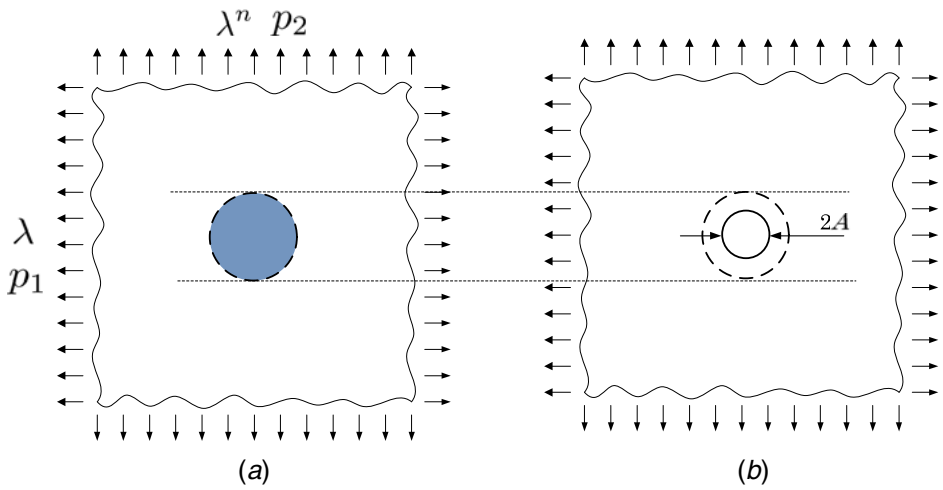

Fig. 2 A membrane under in-plane biaxial loading: (*a*) microscopic strain localization by defect, damage, or material inhomogeneity and (*b*) circular hole as a simplified model

According to the theory of isotropic hyperelastic membranes [67], we can eliminate the 3D effect and treat the problem as a plane stress problem. For this axisymmetric elastostatic problem, the equilibrium equation turns into an ODE about the function $r(R)$,

$$\frac{r}{r'}\frac{df_1}{dR}+f_2=0 \tag{4}$$

where

$$f_1=\left(\frac{\lambda_r}{\lambda_\theta}-\lambda_r^{-3}\lambda_\theta^{-3}\right)\left(\frac{\partial w}{\partial I_1}+\lambda_\theta^2\frac{\partial w}{\partial I_2}\right) \tag{5}$$

$$f_2=\left(\frac{\lambda_r}{\lambda_\theta}-\frac{\lambda_\theta}{\lambda_r}\right)\left(\frac{\partial w}{\partial I_1}+\lambda_r^{-2}\lambda_\theta^{-2}\frac{\partial w}{\partial I_2}\right) \tag{6}$$

with $\lambda_\theta=r(R)/R$ and $\lambda_r=r'(R)$ as the two in-plane principle stretches. w is the strain energy density function in terms of the two invariants of the Cauchy–Green deformation tensor, I_1 and I_2, in $w(I_1, I_2)$. The third invariant is eliminated because of incompressibility. The strain energy density function can also be expressed by the two principal stretches as $\hat{w}(\lambda_1, \lambda_2)$. The energy potentials for a variety of materials are listed in Table 1.

Equation (4) is a nonlinear second-order ODE about $r(R)$ for $R\in[A\ B]$. Instead of matching the stresses or stretches at the remote, we assume the stretch λ_θ at $R=A$ as a given number λ_a and integrate and calculate the corresponding remote stresses and stretches. By assigning λ_a to λ_θ at $R=A$, we have the first boundary condition $r(A)=\lambda_a A$. From the traction-free condition at the hole surface and stretch-stress relation, we have $\lambda_r(A)=\lambda_z(A)=\lambda_a^{-1/2}$, which gives out the second boundary condition $r'(A)=\lambda_a^{-1/2}$. By using the Runge–Kutta method of sixth order [68], and the values of $r(A)$ and $r'(A)$, we solve Eq. (4) for several different hyperelastic materials.

Figure 3 plots the remote equi-biaxial stress p normalized by C versus λ_a for a number of material models. Unlike the spherical cavity under hydrostatic load, for this set of membrane materials, the remote stress has no elastic limit when the stretch at the hole approaches to infinity.

Next, we calculate the normalized driving force, $\mathscr{G}=-d\Pi/[2\pi ACTdA]$ as defined in Eq. (1). By using incompressibility and

Table 1 The strain energy functions for a number of incompressible hyperelastic materials

Material	Energy density function
Neo-Hookean	$w=C(I_1-3)$
Mooney [69]	$w=C_1(I_1-3)+C_2(I_2-3)$
Gent and Thomas [70]	$w=C_1(I_1-3)+C_2\ln\left(\frac{I_2}{3}\right)$
Gent [17]	$w=-CJ_{lim}\ln\left(1-\frac{J_1}{J_{lim}}\right)$, $J_1=I_1-3$
Seitz et al. [19]	$w=CJ_m\left(\exp\left(\frac{J_1}{J_m}\right)-1\right)$, $J_1=I_1-3$
Arruda and Boyce [71]	$w=\mu\sum_{i=1}^{5}\frac{\alpha_i}{\lambda_m^{2i-2}}\left(I_1^i-3^i\right)$, $\alpha_1=\frac{1}{2}$, $\alpha_2=\frac{1}{20}$, $\alpha_3=\frac{11}{1050}$, $\alpha_4=\frac{19}{7000}$, $\alpha_5=\frac{519}{673750}$, $2C=\mu\left(1+\frac{3}{5\lambda_m^2}+\frac{99}{175\lambda_m^4}+\frac{513}{875\lambda_m^6}+\frac{42039}{67375\lambda_m^8}\right)$
Yeoh [72]	$w=\sum_{i=1}^{3}C_i(I_1-3)^i$
Ogden [73]	$w=\sum_{i=1}^{n}\frac{2C_i}{\alpha_i}(\lambda_1^{\alpha_i}+\lambda_2^{\alpha_i}+\lambda_3^{\alpha_i}-3)$

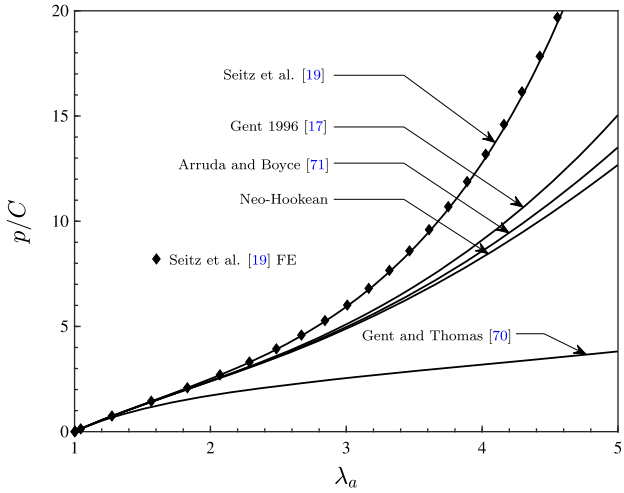

Fig. 3 Remote equi-biaxial tension versus the hole stretch ratio: Seitz et al. [19], $J_m=20$; Gent [17], $J_{lim}=92$; Gent and Thomas [70], $C_1=0.5C$ and $C_2=1.5C$; and Arruda and Boyce [71], $\lambda_m=7$

assume $B>>A$, as derived in Appendix, we have

$$\bar{\mathscr{G}}(\lambda)=-\frac{1}{2\pi ATC}\frac{dU}{dA}=\frac{1}{2}\lambda\bar{w}'(\lambda)+\bar{W}(\lambda) \tag{7}$$

In Eq. (7), $\bar{w}'$ is the first derivative of the strain energy density at remote where the principal stretches are $(\lambda,\lambda,\lambda^{-2})$, normalized by C. $\bar{W}$ is the work done by a traction acting on the hole to pull it back from λ_a to the remote stretch λ, normalized by πA^2TC.

As shown in Eq. (7), the normalized driving force for an infinite membrane depends on the remote stretch λ or normalized remote stress p/C. Figure 4 shows the normalized driving force versus the normalized remote tension p/C for several hyperelastic material models. All curves follow the same path for small load and then diverge when p is roughly $2C$. The normalized driving forces for I_1-materials whose energy functions just depend on I_1 (neo-Hookean, Gent [17] and Seitz et al. [19]) are very close, unlike the I_1-I_2-materials, whose energy functions depend on both I_1 and I_2 (Mooney [69] and Gent and Thomas [70]). For the former group, the normalized driving force linearly depends on the remote tension when $p/C>2$, with the slope of about $\pi/2$.

Consider all the I_1-materials in Fig. 4, although these materials give quite different near-field solutions around the hole, the

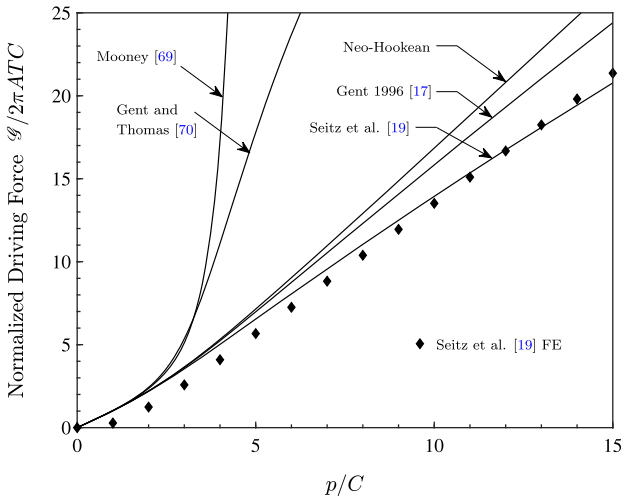

Fig. 4 Normalized driving force for hole growth versus equi-biaxial remote tension

closeness of the normalized driving force indicates that the relaxed strain energy in growth is mainly from the intermediate and far field, in which the normalized fields are similar at moderate or small stretch ratios. The similar result occurs in fracture mechanics, in which the details of the plastic deformation near a crack tip have a weak influence on the energy-release rate of a crack in an infinite body. However, the normalized driving force is quite different for a material whose energy function depends on I_2 as well, partly because it needs two material constants to fit its material behavior even at moderate stress level.

The above results from the ODE can be used as a benchmark to cross check the results from the finite element for nonlinear large deformation. In Figs. 3 and 4, the finite element results, for the material model by Seitz et al. [19], are also plotted (as marks). Results from ODE and FEM are close, indicating that at least for the equal-biaxial loading case, our numerical treatment has no convergence issue.

To show the effect of the shape of the defect, driving force is calculated for a sharp crack of size $2A_c$ using FEM. To compare with the previous results, we define and normalize the driving force in the same way as in Eq. (1) using the size of an imaginary circular hole, $A = 2A_c/\pi$, that gives the same surface area as the crack [47,48]. The material is neo-Hookean. Figure 5 shows the normalized driving force for the crack calculated directly from FEM results (dashed line) together with that of a circular hole of the equivalent size (solid line). For comparison, normalized J-integral of the crack from FEM and the estimation by Yeoh [74] are also plotted. We expect that the driving force for the defect of other shapes is between the solid line and those dashed lines. For these curves, the normalized driving force linearly depends on the remote tension except when the load is small. Yeoh [74] estimated the slope to be $\pi/2$, which is also shown in the graph and fairly represents the driving force–load relation.

2.2 General Biaxial Load. For the cases of general biaxial loading, we use the finite element method to solve the stress and deformation fields. We follow the same procedure as the equi-biaxial case to obtain the driving force, as described in Appendix.

First, we consider the neo-Hookean material. Figure 6 depicts the normalized driving force versus the normalized remote stress p for the neo-Hookean material under different biaxialities n, where $p = p_1$ is a leading principal stress, the larger one of the two principle stresses. As expected, the equi-biaxial load, $n = 1$, yields the highest driving force. For loadings with biaxialities between $n = -0.5$ (uniaxial) and $n = 0$ (pure shear), the driving force values are close. As shown in the figure, to have the same

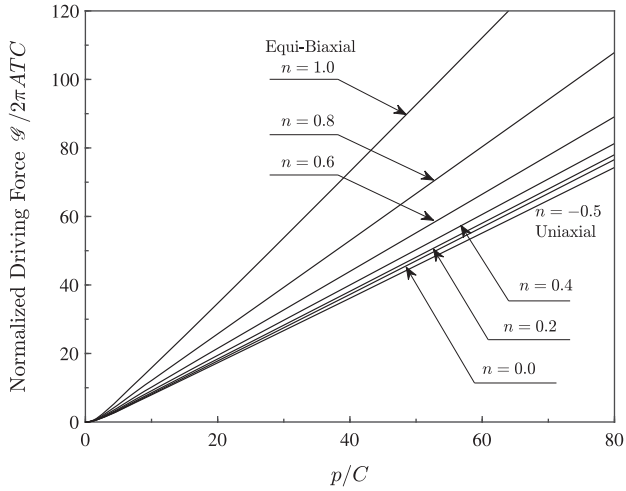

Fig. 6 Normalized driving force versus the larger remote stress for the neo-Hookean material under biaxial loadings of different biaxialities

driving force, loads with smaller biaxiality require a larger leading principal stress p.

In addition, same as in equi-biaxial loading, the normalized driving force linearly depends on remote tension when $p/C > 2$. The extension of this straight line from the large load to the small load region gives a small intercept with the horizontal axis. If we neglect that intercept, for sufficiently large $\bar{p} = p/C$,

$$\frac{\bar{\mathscr{G}}}{\bar{p}} = \gamma(n) \tag{8}$$

in which γ is a number just depending on the biaxiality n as shown in Fig. 7. For n, from −0.5 to 0.5, γ is roughly 1. The numerical results can be fitted by an exponential curve,

$$\gamma(n) = 0.01795e^{4n} + 0.9426 \tag{9}$$

For all the other I_1-materials in Fig. 4, the driving force–remote stress relation and their dependence on biaxility is similar to the neo-Hookean materials. However, for I_1-I_2-materials, the relation between driving force and remote load and its dependency on biaxiality are completely different from I_1-materials. For example, Fig. 8 shows the driving force versus remote load under different biaxilities for Gum Stock, which fits the Mooney's material model [69]

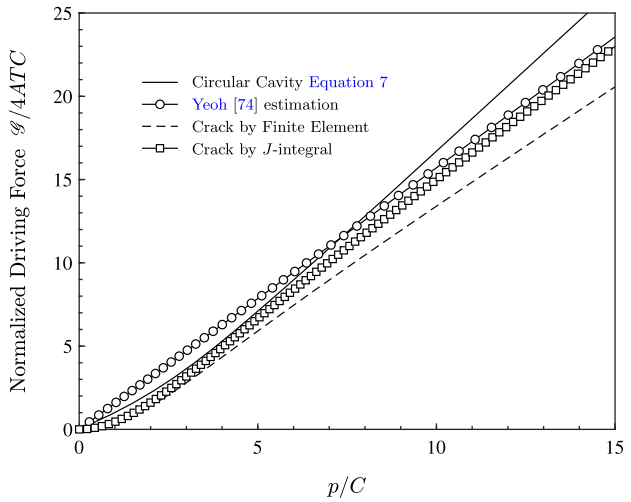

Fig. 5 Normalized driving force for the crack growth compared with that of a hole of same surface area

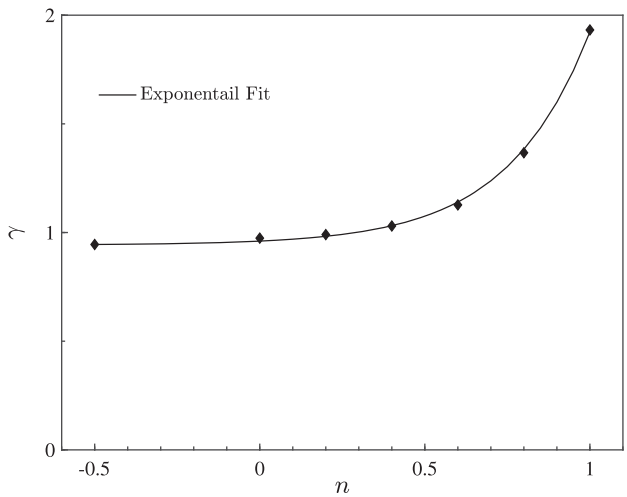

Fig. 7 $\gamma(n)$, as defined in Eq. (8), versus biaxiality for the neo-Hookean material

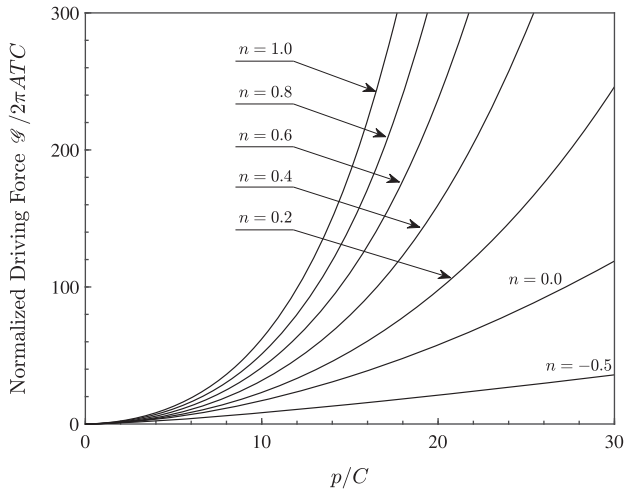

Fig. 8 Normalized driving force versus the remote stress for Mooney's material with $C_1/C = 0.724$ and $C_1/C = 0.276$ in different biaxialities

with $C_1 = 0.1205$ MPa and $C_2 = 0.0460$ MPa. The linear relation between the driving force and the remote stress found in I_1--materials does not fit for this material. Also, unlike in the neo-Hookean material where the driving forces for small biaxialities (between -0.5 and 0.5) are close, and for this material, the driving force is more sensitive to biaxiality when it is smaller.

3 Energy-Based Strength Theory for Membrane

Next we consider the condition under which the hole grows irreversibly. The mechanical energy reduction associated with the hole growth is $-d\Pi = 2\pi TC\bar{\mathcal{G}}AdA$, where $\bar{\mathcal{G}}$ is calculated in Sec. 2. As mentioned earlier in Sec. 1, when a hole is small enough and irreversibly grows, the energy is dissipated all around the defect. The energy needed for the hole growth, including dissipative energy and reverse healing energy (if there is any), is $2\pi T\Gamma_p AdA$. Consequently, the condition for hole growth is

$$\bar{\mathcal{G}} = \frac{\Gamma_p}{C} \tag{10}$$

which is the same as that in the hydrostatic tension case [48]. Thus, by using Figs. 3 and 4, one could estimate the volume process energy Γ_p from the loading parameters, λ or p, at the critical state. Using the obtained value and the calculated driving forces in Figs. 6 and 8, we can determine the critical load at other biaxialities. This energy approach connects the reduction of elastic energy in the whole body to the energy barrier for the growth in the near-field around the defect. All the details of dissipation mechanisms and the ultimate stretchability [25,44] are embedded in the energy barrier Γ_p. In the following, we first take neo-Hookean and Mooney's materials as two examples to show that we can predict the critical load for general biaxial loading by only using the data in the equi-biaxial loading experiment. Γ_p can just be used as an intermediate property to connect loadings of different biaxialities. It can be replaced by the directly measurable critical stress or stretch at equi-biaxial loading. Afterward, we derive the similar failure criteria for material models by Yeoh [72] and Ogden [73]. The results are compared with the experimental data by Hamdi et al. [66].

3.1 Neo-Hookean and I_1-Materials. Consider the neo-Hookean material as an example of I_1-materials. Let $\bar{p}_{cr}$ be the critical value of p_1 normalized by C, where p_1 is the leading principal stress, the larger one of the two principal stresses. Combining Eqs. (8)–(10), we have

$$\frac{p_{cr}}{p^e_{cr}} = \frac{\gamma(1)}{\gamma(n)} = \frac{1.92}{0.018e^{4n} + 0.94} \tag{11}$$

where p^e_{cr} is the critical stress in the equi-biaxial case. To obtain the relation in the principal stretch plane, we use the constitutive relation for the plane stress condition:

$$p_1 = \lambda_1 \frac{\partial \hat{w}}{\partial \lambda_1} \tag{12}$$

The $\hat{w}(\lambda_1, \lambda_2)$ is the modified strain density w function for incompressible material under plane stress. In fact, one can eliminate the hydrostatic pressure by setting the principal stresses as $p_1 - p_3$ and $p_2 - p_3$, and as we know $p_3 \approx 0$ [21]. Next, using the constitutive relation of Eq. (12), we rewrite Eq. (11) for Neo-Hookean in term of principal stretch. When λ_{cr} is much larger than 1,

$$\frac{\lambda_{cr}}{\lambda^e_{cr}} = \sqrt{\frac{\gamma(1)}{\gamma(n)}} = \frac{1.39}{\sqrt{0.018e^{4n} + 0.94}} \tag{13}$$

The value of Γ_p for natural rubber is estimated to be between 60 and 100 MPa. Take the initial elastic modulus E as 2 MPa, we have the value of Γ_p/C about 180–300. Given these typical values of Γ_p/C, Fig. 9 depicts the failure "surface" of the neo-Hookean material in principal stretch and principal stress planes, respectively. The critical stretches and critical stresses are normalized by the corresponding values of the equi-biaxial case. As observed in Fig. 9 the value of Γ_p/C itself has a weak influence on the shape of the failure surface in principal stresses and principal stretches normalized by equi-biaxial critical values. The surface approximately retains the shape of a circle with the radius of $\sqrt{2}$ in the principal stretch plane. While in the principle stress plane, the failure surface is close to a straight line. Finally, it is worth noting again that the approximations in Eqs. (11) and (13) are based on the assumption that the critical stretch λ_{cr} is much larger than 1.

We also calculate the failure surfaces for other I_1-materials. The results are the same as what depicted in Fig. 9 (two such examples are illustrated in Figs. 13 and 14). The failure surface is close to a straight line in the principal stress plane and a circle in the principal stretch plane. The failure surface in the principal stretch plane is close to $\lambda_1^2 + \lambda^2 = 2(\lambda^e_{cr})^2$. This is very close to the critical I_1 criterion proposed by Gent [17], because λ_3^2 is negligible at the failure. However, it is worth noting that the critical I_1 criterion is not applicable to general 3D multi-axial loading cases, in which the hydrostatic stress plays a significant role in the rupture but has no effect on the macroscopic deformation.

3.2 Mooney's Material. Unlike I_1-material, the relation between the driving force and the remote stress for Mooney's material (Fig. 8) is not close to linear. The failure surface is shown in Fig. 10 for values of Γ_p/C between 180 and 300, where $C = C_1 + C_2$ for Mooney's material. The failure surface in the principal stretch plane (Fig. 10(*a*)) is completely different from a circle and cannot be fitted by the critical I_1 criterion. It also shows that the critical normalized stress or stretch at small values of n are relatively large. This is due to the dependence of energy density function w on I_2, which is approximately λ^4 for the equi-biaxial case and about 2λ for the uniaxial case when $\lambda >> 1$, where λ is the larger one of the two principal stretches. The big drop in energy density from equi-biaxial to uniaxial causes the large raise in the critical load from equi-biaxial to uniaxial, as shown in Fig. 10. Another important observation is that in the principal stress plane in Fig. 10(*b*), the failure surface again approximately forms a straight line in the principal stress plane.

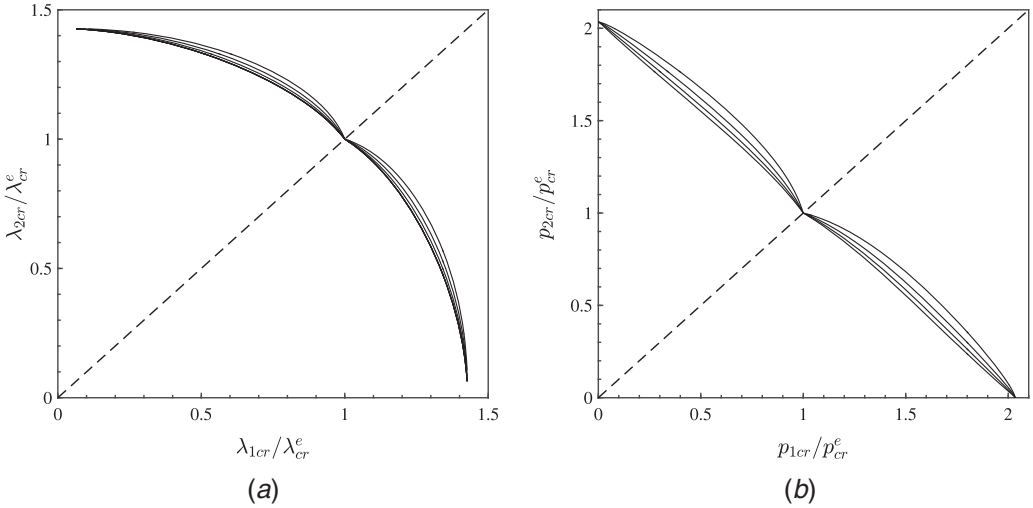

Fig. 9 The failure criteria of the membrane made of the neo-Hookean material, for Γ_p/C 180 ~ 300: (*a*) in principle stretch plane and (*b*) in principle stress plane

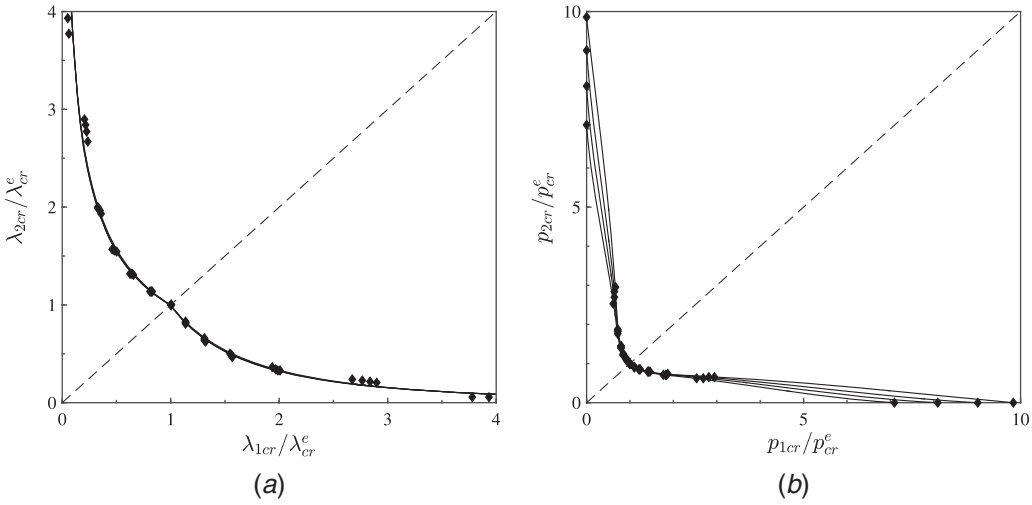

Fig. 10 The failure criteria of the membrane made of Gum-Stock mentioned in Ref. [69], for Γ_p/C 180 ~ 300: (*a*) in principle stretch plane and (*b*) in principle stress plane. Marks are calculated values and solid lines are fitted curves.

3.3 Natural Rubber and Styrene–Butadiene Rubber. Hamdi et al. [66] conducted a series of biaxial experiments on thin membranes made of two elastomers, NR and styrene–butadiene rubber (SBR). They proposed the Yeoh's model [72] for NR and the Ogden's model [73] for SBR. The fitting parameters of the materials are listed in Table 2. In the experiments, they measured the critical stretch ratios of the membranes under different biaxialities n: $n = 1$, 0.88, 0.82, 0.81 for NR, $n = 1$, 0.88, 0.82, 0.68 for SBR, and $n = -0.5$ (uniaxial stress state) for both. The measured values of critical stresses by Hamdi et al. [66] were scattered with a relatively large deviation, indicating the sensitivity to the samples or the conditions of testing.

Table 2 The material properties of NR and SBR prepared by Hamdi et al. [66]

Properties	C_1 (MPa)	C_2 (MPa)	C_3 (MPa)	α_1	α_2
Yeoh's for NR	0.298	0.014	1.6×10^{-4}		
Ogden's for SBR	0.319	−0.0125		3.03	−2.35

The rupture in Hamdi et al.'s [66] experiments might start with the first stage of defect growth, which is triggered by a small-scale defect, i.e., highly strained zone. At this stage, the drastic change might not be observed because the process is localized around the defect and does not induce significant change in the remote stress or stretch. However, when the defect reaches the characteristic size, the transition to cracking is unstable and the membrane ruptures.

By using Yeoh's model for NR and Ogden's for SBR, we calculate the driving force versus remote stretch for the same biaxilities as in the experiments. Figures 11 and 12 show the normalized driving force versus the leading principal stretch λ, the larger one of the two principal stretches, for NR and SBR, respectively. In these two graphs, the measured critical stretches and the corresponding driving forces are marked on the curves for different n values. Different from our ideal model, the critical driving force from the experiments varies with biaxiality for both NR and SBR. This could be due to the statistical variation in the tests or the idealistic assumptions we make in the model. For example, energy dissipation is not exactly uniform around the defect, especially when biaxiality n is small. Also, a slight deviation of the measured

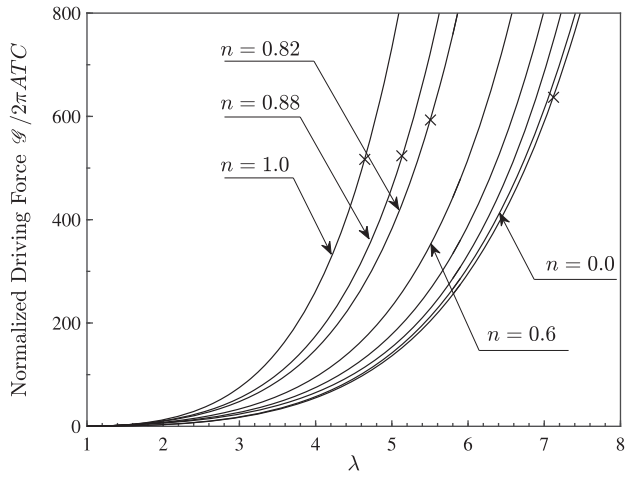

Fig. 11 Normalized driving force for the hole growth versus the larger remote stretch for NR. Marks of "×" show the critical points from experiments.

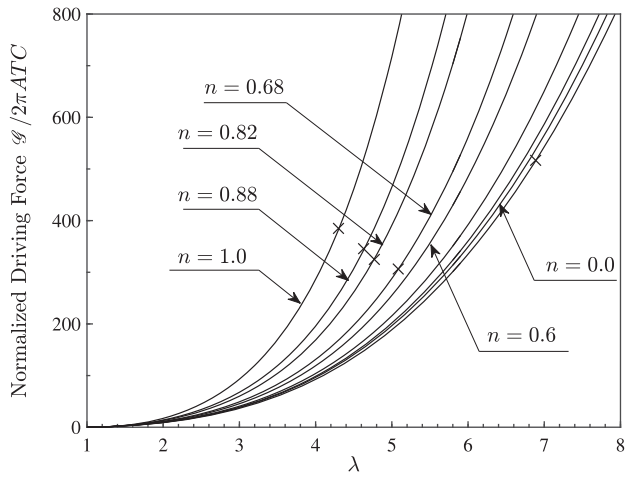

Fig. 12 Normalized driving force for the hole growth versus the larger remote stretch for SBR. Marks of "×" show the critical points from experiments.

stretch ratio in experiment could give large difference in the normalized driving force. However, this should not be a big concern for us, because Γ_p here is just used as an intermediate value. When we write the failure condition in terms of the principal stretches, as long as Γ_p is above a certain value, its variation only causes small change in the critical stretch. However, if we express the failure condition in terms of stress, the change of Γ_p causes the same order of change in p_{cr}/C. This is what was revealed in Hamdi et al.'s experiments that the measured stresses at failure had very large deviation. We suggest to pick the lower measured value as the limit load for practical applications.

Next, we use the critical driving force of NR and SBR in the equi-biaxial loading to predict the critical stretches and critical stresses at different load biaxialities, including those in the experiments. Thus, we can make a direct comparison between the predicted critical load and the experiment. Figures 13 and 14 show the failure surfaces for NR and SBR, respectively, in (*a*) the principal stretch plane and in (*b*) the principal stress plane. The diamonds are the predictions from Eq. (10). Since we use the equi-biaxial data to obtain Γ_p/C, the predicted result exactly lies on top of the experimental data point of the equi-biaxial loading. As predicted for the neo-Hookean solid, for the materials whose energy functions only depend on I_1, the failure envelope is approximately a circle in the principal stretch plane and roughly a straight line in the principal stress plane. The approximate fit to the failure condition in stretch plane (diamonds) is

$$\left(\frac{\lambda_1}{\lambda_{cr}^e}\right)^\alpha + \left(\frac{\lambda_2}{\lambda_{cr}^e}\right)^\alpha = 2 \tag{14}$$

where $\alpha = 1.8$ for the two materials. This result again verifies the conclusion we obtained in Sec. 3.1: for I_1 materials, the failure surface in the stretch plane is close to a circle. For simplicity, we can just set $\alpha = 2$ in Eq. (14). Again, same as the other materials, the failure surface in the principal stress plane is close to a straight line, as shown in Figs. 13(*b*) and 14(*b*).

It should be pointed out that our numerical results (diamond) and the fitting curve only use one data point from the equi-biaxial test, but obtain the critical conditions close to the experimental results for other biaxialities. In Figs. 13(*b*) and 14(*b*), we also note the large deviation of the experimental data in critical stresses. Since the biaxilities in the biaxial tests in the study by Hamdi et al. are between 0.81 and 1 for NR and 0.68 and 1 for SBR, it is hard to tell how good the prediction is for other small biaxialities. One important check point is the extreme case of uniaxial loading, at

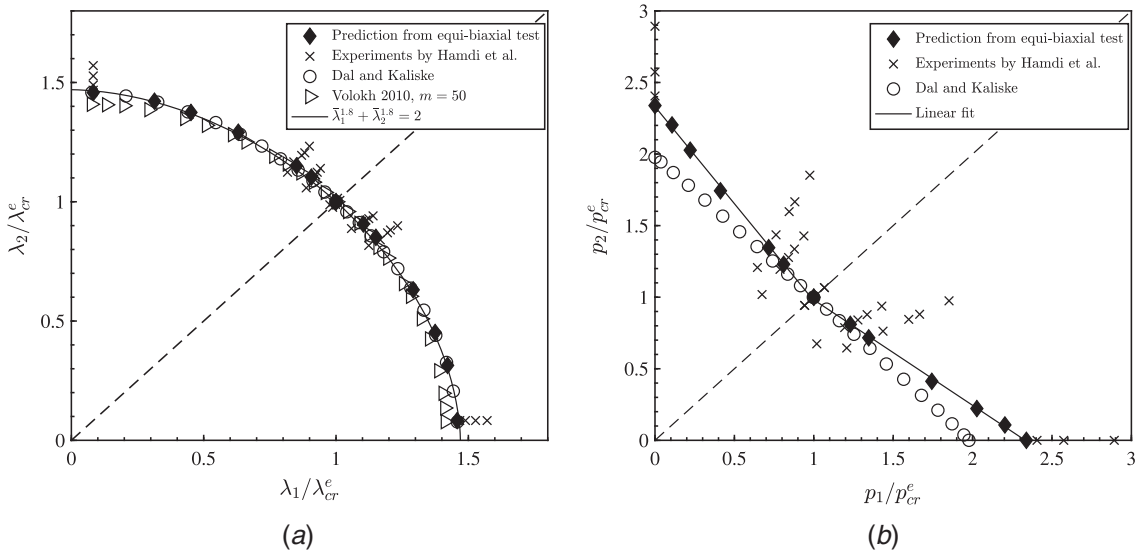

Fig. 13 The failure criteria of NR membrane: (*a*) in principle stretch plane and (*b*) in principle stress plane. Marks of "×" are from the experiment.

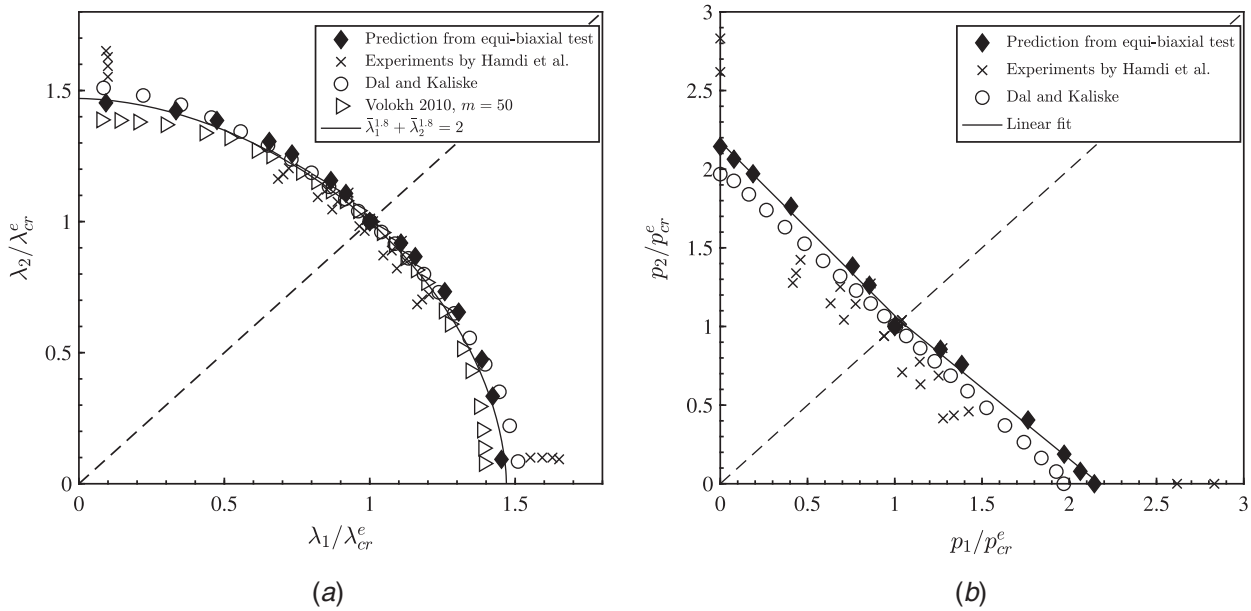

Fig. 14 The failure criteria of SBR membrane: (*a*) in principle stretch plane and (*b*) in principle stress plane. Marks of "×" are from the experiment.

which the model here is supposed to work worst due to the assumption of even energy dissipation around the hole. Yet, for both materials, we capture the lower experimental values in uniaxial loading tests by using the equi-biaxial data alone. This underestimation is acceptable from the safe design point of view.

The results by Volokh [39] and Dal and Kaliske [43] are also marked in the two failure surfaces for NR and SBR. Their approaches were based on constitutive models with more material constant.

4 Conclusion

We proposed two defect growth modes in Ref. [48], one is omni-directional dissipation mode and the other is cracking. There is a characteristic material length that separate the two modes. Defect grows in the first mode when its size is smaller than the characteristic size and grows by cracking when its size is larger. In the both modes, we use the Griffith type energy criterion to determine the conditions for the defect growth. It results in the size-independent critical loading condition for the first growth mode as in the traditional strength theory. For the second growth mode, it follows in the scope of fracture mechanics. The results show that strength theory and fracture theory can be united under one theoretical framework. This paper uses this fundamental principle to study the rupture of membrane under biaxial loading.

Assuming strain localization as the precursor for final rupture, mathematically, we model any preexisting defect or strain localization site as a through-thickness hole in the membrane. We further assume that the hole size is smaller than the characteristic size for highly stretchable thin membranes and consider the first growth mode of the defect. We obtain the driving force of the defect growth for a group of materials under the equi-biaxial loading. The results for the general biaxial loading is obtained from FEM calculations. We use volume process energy Γ_p, which represents energy dissipation in a variety of dissipative mechanisms, to characterize the energy barrier against the growth. Defect grows when the elastic energy relaxed in growth is larger than the energy barrier, mainly the dissipative energy is associated with the growth process. We ignore hardening and assume a constant Γ_p. If there is hardening due to any physical mechanism, we may treat Γ_p in our formulation as the maximum value that the material can obtain. Hardening effect may change the initial profile of the curve in Fig. 1, but it will not affect our final results. We further replace the material parameter Γ_p by the critical stress or stretch in equi-biaxial and derive the failure conditions in terms of principal stretches or principal stresses. Through calculations for several I_1-materials, we find that the failure surfaces in the principal stretch plane are about the same for all I_1-materials. The failure condition can be approximated by

$$\lambda_1^2 + \lambda_2^2 = 2(\lambda_{cr}^e)^2 \tag{15}$$

This result is also close to the I_1 criterion because λ_3^2 is negligible at failure. However, we should be aware that the I_1 criterion is not applicable for a three-dimensional solid under general multi-axial loading. We also calculate the failure conditions for I_1-I_2-materials whose energy density depends on both I_1 and $I_1 2$. The results are completely different from the I_1 materials. The failure surface cannot be fitted by a circle, and the I_1 criterion is not applicable for these materials. The critical stress in uniaxial loading is one order higher than that in equi-biaxial loading.

One important observation is that, for any materials we studied, the failure surface in the principal stress plane is close to a straight line. For a practical purpose, we may approximate the linear relation by

$$p_1 + \left(\frac{p_{cr}^u}{p_{cr}^e} - 1\right) p_2 = p_{cr}^u \quad (p_1 \geq p_2) \tag{16}$$

where p_{cr}^u and p_{cr}^e are the critical stresses in uniaxial loading and biaxial loading cases, respectively. *Instead of doing FEM calculation, one can simply measure these two critical stresses and get the failure condition for general biaxial loading.*

We used the experimental data for natural rubber and styrene-butadiene rubber to check our theoretical predictions. Only by using the critical stretch or stress in the equi-biaxial loading case, we can predict the critical stretches or stresses for other biaxial loadings with different biaxialities. The predictions are in good agreement with the experimental data on NR and SBR.

Acknowledgment

This work was supported by the National Natural Science Foundation of China (Nos. 11525210, 11621062, and 91748209), the Fundamental Research Funds for the Central Universities, and PSC CUNY Research Foundation (TRADA-45-324).

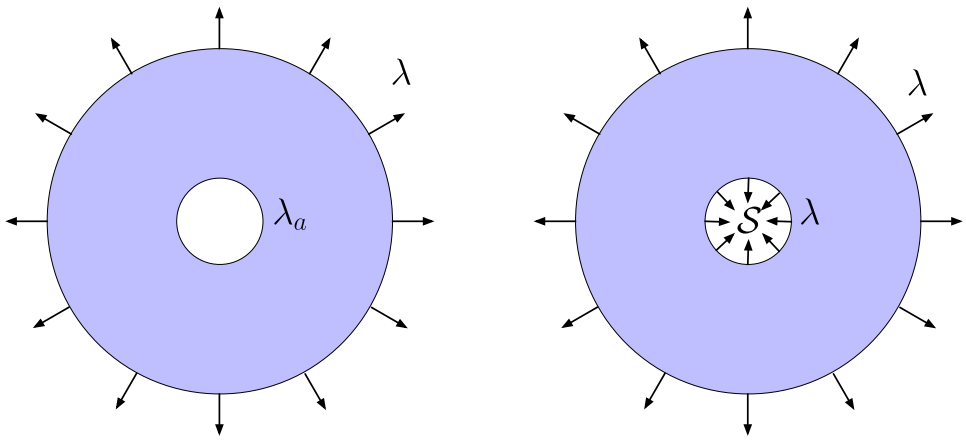

Fig. 15 (*a*) The current configuration of the membrane under the remote stretch of λ and cavity stretch λ_a. (*b*) The traction $\mathcal{S}$ is stretching the cavity to λ generating a uniform deformation

Appendix: Normalized Driving Force $\bar{\mathcal{G}}(\lambda)$

Consider the membrane in Fig. 15(*a*), if we pull the surface of the hole back from the stretch λ_a at traction-free state to λ, we obtain the state in Fig. 15(*b*), which is uniformly deformed with principal stretches $(\lambda, \lambda, \lambda^{-2})$. Thus, we have the strain energy U of the configuration in Fig. 15(*a*):

$$U = U_{ref} - W \tag{A1}$$

where U_{ref} is the strain energy of configuration in Fig. 15(*b*) and W is the work done by the traction at the hole surface in the pulling back process. Let $\mathcal{S}(\xi, \bar{B})$ be the nominal normal stress at the surface of the hole normalized by C. It depends on the circumferential stretch at the hole and the normalized size of the membrane $\bar{B} = B/A$. Thus,

$$W = 2\pi A^2 TC \int_{\lambda}^{\lambda_a} \mathcal{S}(\xi, \bar{B})\, d\xi \tag{A2}$$

and

$$U_{ref} = \pi T(B^2 - A^2) w(\lambda) \tag{A3}$$

where w is the strain energy density. Assume the load is displacement controlled (λB is constant) and the volume is preserved ($B^2 - A^2$ is constant), and hence,

$$\frac{dU_{ref}}{dA} = \pi T(B^2 - A^2) w'(\lambda) \frac{d\lambda}{dA} \tag{A4}$$

$$\frac{d\lambda}{dA} = \frac{d}{dA}\frac{b}{B} = -b\frac{1}{B^2}\frac{dB}{dA} = -b\frac{1}{B^2}\frac{A}{B} = -\lambda\frac{A}{B^2} \tag{A5}$$

Combining the last two equations, we obtain

$$\frac{1}{2\pi ATC}\frac{dU_{ref}}{dA} = -\frac{1}{2}\lambda \bar{w}'(\lambda)\left(1 - \frac{1}{\bar{B}^2}\right) \tag{A6}$$

Taking derivative of Eq. (A2), we have

$$\frac{dW}{dA} = 4\pi ATC \int_{\lambda}^{\lambda_a} \mathcal{S}(\xi, \bar{B})\, d\xi + 2\pi A^2 TC \times \left[-\mathcal{S}(\lambda, \bar{B})\frac{d\lambda}{dA} + \frac{d\bar{B}}{dA}\int_{\lambda}^{\lambda_a} \frac{\partial \mathcal{S}(\xi, \bar{B})}{\partial \bar{B}}\, d\xi \right] \tag{A7}$$

and

$$\frac{1}{2\pi ATC}\frac{dW}{dA} = 2\int_{\lambda}^{\lambda_a} \mathcal{S}(\xi, \bar{B})\, d\xi + \frac{\mathcal{S}\lambda}{\bar{B}^2} + \left(\frac{1}{\bar{B}} - \bar{B}\right)\int_{\lambda}^{\lambda_a} \frac{\partial \mathcal{S}(\xi, \bar{B})}{\partial \bar{B}}\, d\xi \tag{A8}$$

Referring to Eq. (A1) and collecting Eqs. (A6) and (A8)

$$\frac{1}{2\pi ATC}\frac{dU}{dA} = -\frac{1}{2}\lambda \bar{w}'(\lambda)\left(1 - \frac{1}{\bar{B}^2}\right) - 2\int_{\lambda}^{\lambda_a} \mathcal{S}(\xi, \bar{B})\, d\xi - s\lambda^2\frac{1}{\bar{B}^2} - \left(\frac{1}{\bar{B}} - \bar{B}\right)\int_{\lambda}^{\lambda_a} \frac{\partial \mathcal{S}(\xi, \bar{B})}{\partial \bar{B}}\, d\xi \tag{A9}$$

For linear elasticity, we know $\partial \mathcal{S}(\xi, \bar{B})/\partial \bar{B}$ is on the order of $1/\bar{B}^3$. For general hyperelastic material, it is also evident to verify that $\partial \mathcal{S}(\xi, \bar{B})/\partial \ln \bar{B}$ vanishes as $\bar{B} \to \infty$. Hence, when $\bar{B} \to \infty$

$$-\frac{1}{2\pi ATC}\frac{dU}{dA} = \frac{1}{2}\lambda \bar{w}'(\lambda) + 2\int_{\lambda}^{\lambda_a} \mathcal{S}(\xi)\, d\xi \tag{A10}$$

The integral in the second term of Eq. (A10) is in Eq. (A2), and thus,

$$\bar{\mathcal{G}}(\lambda) = -\frac{1}{2\pi ATC}\frac{dU}{dA} = \frac{1}{2}\lambda \bar{w}'(\lambda) + \bar{W}(\lambda) \tag{A11}$$

where

$$\bar{W}(\lambda) = \frac{W}{\pi A^2 TC} = \int_{\lambda}^{\lambda_a} \mathcal{S}(\xi, \bar{B} = \infty)\, d\xi \tag{A12}$$

The result for general biaxial loading is similar; the first term of the right-hand side of Eq. (A11) turns into $\frac{1}{2}(\lambda_1(\partial \bar{w}/\partial \lambda_1) + \lambda_2(\partial \bar{w}/\partial \lambda_2))$, and the second term is still the normalized work done by the corresponding traction in pulling the hole from the traction-free state to the uniformly stretched state, which is also the energy difference between the two states.

References

[1] Gent, A., and Lindley, P., 1959, "Internal Rupture of Bonded Rubber Cylinders in Tension," Proc. Roy. Soc. Lond. Math. Phys. Sci., **249**, pp. 195–205.
[2] Gent, A., 1990, "Cavitation in Rubber: A Cautionary Tale," Rubber Chem. Technol., **63**(3), pp. 49–53.
[3] Denecour, R., and Gent, A., 1968, "Bubble Formation in Vulcanized Rubbers," J Polym. Sci. B Polym. Phys., **6**(11), pp. 1853–1861.
[4] Sekhar, N., and Van Der Hoff, B., 1971, "Cavity Formation on Elongation in Filled Elastomers," J. Appl. Polym. Sci., **15**(1), pp. 169–182.
[5] Gent, A., and Tompkins, D., 1969, "Nucleation and Growth of Gas Bubbles in Elastomers," J. Appl. Phys., **40**(6), pp. 2520–2525.

[6] Gent, A., and Tompkins, D., 1969, "Surface Energy Effects for Small Holes or Particles in Elastomers," J. Polym. Sci. B Polym. Phys., **7**(9), pp. 1483–1487.
[7] Gent, A., and Tompkins, D., 1970, "Surface Energy Effects for Small Holes or Particles in Elastomers," Rubber Chem. Technol., **43**(4), pp. 873–877.
[8] Crosby, A. J., Shull, K. R., Lakrout, H., and Creton, C., 2000, "Deformation and Failure Modes of Adhesively Bonded Elastic Layers," J. Appl. Phys., **88**(5), pp. 2956–2966.
[9] Bayraktar, E., Bessri, K., and Bathias, C., 2008, "Deformation Behaviour of Elastomeric Matrix Composites Under Static Loading Conditions," Eng. Fracture Mech., **75**(9), pp. 2695–2706.
[10] Belayachi, N., Benseddiq, N., Naït-Abdelaziz, M., and Hamdi, A., 2008, "On Cavitation and Macroscopic Behaviour of Amorphous Polymer-Rubber Blends," Sci. Technol. Adv. Mater., **9**(2), p. 025008.
[11] Cristiano, A., Marcellan, A., Long, R., Hui, C.-Y., Stolk, J., and Creton, C., 2010, "An Experimental Investigation of Fracture by Cavitation of Model Elastomeric Networks," J. Polym. Sci. B Polym. Phys., **48**(13), pp. 1409–1422.
[12] Ilseng, A., Skallerud, B. H., and Clausen, A. H., 2017, "An Experimental and Numerical Study on the Volume Change of Particle-Filled Elastomers in Various Loading Modes," Mech. Mater., **106**, pp. 44–57.
[13] Poulain, X., Lefèvre, V., Lopez-Pamies, O., and Ravi-Chandar, K., 2017, "Damage in Elastomers: Nucleation and Growth of Cavities, Micro-Cracks, and Macro-Cracks," Int. J. Fracture, **205**(1), pp. 1–21.
[14] Bueche, F., and Halpin, J., 1964, "Molecular Theory for the Tensile Strength of Gum Elastomers," Rubber Chem. Technol., **37**(4), pp. 808–817.
[15] Kawabata, S., 1973, "Fracture and Mechanical Behavior of Rubber-Like Polymers Under Finite Deformation in Biaxial Stress Field," J. Macromol. Sci. B, **8**(3–4), pp. 605–630.
[16] Smith, T. L., and Rinde, J. A., 1969, "Ultimate Tensile Properties of Elastomers. v. Rupture in Constrained Biaxial Tensions," J. Polym. Sci. B Polym. Phys., **7**(4), pp. 675–685.
[17] Gent, A., 1996, "A New Constitutive Relation for Rubber," Rubber Chem. Technol., **69**(1), pp. 59–61.
[18] Brown, K., and Creton, C., 2002, "Nucleation and Growth of Cavities in Soft Viscoelastic Layers Under Tensile Stress," Eur. Phys. J. E. Soft Matter, **9**(1), pp. 35–40.
[19] Seitz, M. E., Martina, D., Baumberger, T., Krishnan, V. R., Hui, C.-Y., and Shull, K. R., 2009, "Fracture and Large Strain Behavior of Self-Assembled Triblock Copolymer Gels," Soft Matter, **5**(2), pp. 447–456.
[20] Lev, Y., and Volokh, K. Y., 2016, "On Cavitation in Rubberlike Materials," J. Appl. Mech., **83**(4), p. 044501.
[21] Liu, J., Chen, Z., Liang, X., Huang, X., Mao, G., Hong, W., Yu, H., and Qu, S., 2018, "Puncture Mechanics of Soft Elastomeric Membrane With Large Deformation by Rigid Cylindrical Indenter," J. Mechan. Phys. Solids, **112**, p. 458.
[22] Griffith, A. A., 1921, "VI. The Phenomena of Rupture and Flow in Solids," Phil. Trans. R. Soc. Lond. A, **221**(582–593), pp. 163–198.
[23] Rivlin, R., and Thomas, A. G., 1953, "Rupture of Rubber. I. Characteristic Energy for Tearing," J. Polym. Sci., **10**(3), pp. 291–318.
[24] Williams, M., and Schapery, R., 1965, "Spherical Flaw Instability in Hydrostatic Tension," Int. J. Fracture Mech., **1**(1), pp. 64–72.
[25] Lake, G., and Thomas, A., 1967, "The Strength of Highly Elastic Materials," Proc. Roy. Soc. Lond. Math. Phys. Sci., **300**, pp. 108–119.
[26] Smith, T. L., 1970, "Rupture Processes in Polymers," Pure Appl. Chem., **23**(2–3), pp. 235–254.
[27] Gent, A., and Wang, C., 1991, "Fracture Mechanics and Cavitation in Rubber-Like Solids," J. Mater. Sci., **26**(12), pp. 3392–3395.
[28] Dollhofer, J., Chiche, A., Muralidharan, V., Creton, C., and Hui, C., 2004, "Surface Energy Effects for Cavity Growth and Nucleation in an Incompressible Neo-Hookean Material–Modeling and Experiment," Int. J. Solids Struct., **41**(22), pp. 6111–6127.
[29] Nait-Abdelaziz, M., Zairi, F., Qu, Z., Hamdi, A., and Hocine, N. A., 2012, "J Integral as a Fracture Criterion of Rubber-Like Materials Using the Intrinsic Defect Concept," Mech. Mater., **53**, pp. 80–90.
[30] Cantournet, S., Layouni, K., Laiarinandrasana, L., and Piques, R., 2014, "Experimental Investigation and Modelling of Compressibility Induced by Damage in Carbon Black-Reinforced Natural Rubber," CR Mécanique, **342**(5), pp. 299–310.
[31] Movahed, P., Kreider, W., Maxwell, A. D., Hutchens, S. B., and Freund, J. B., 2016, "Cavitation-Induced Damage of Soft Materials by Focused Ultrasound Bursts: A Fracture-Based Bubble Dynamics Model," J. Acoust. Soc. Amer., **140**(2), pp. 1374–1386.
[32] Drass, M., Schneider, J., and Kolling, S., 2018, "Novel Volumetric Helmholtz Free Energy Function Accounting for Isotropic Cavitation at Finite Strains," Mater. Design, **138**, pp. 71–89.
[33] Mishra, S., Lacy, T. E., and Kundu, S., 2018, "Effect of Surface Tension and Geometry on Cavitation in Soft Solids," Int. J. Non-Linear Mech., **98**, pp. 23–31.
[34] Baer, E., Hiltner, A., and Keith, H., 1987, "Hierarchical Structure in Polymeric Materials," Science, **235**(4792), pp. 1015–1022.
[35] Klein, P., and Gao, H., 1998, "Crack Nucleation and Growth as Strain Localization in a Virtual-Bond Continuum," Eng. Fracture Mech., **61**(1), pp. 21–48.
[36] Gao, H., and Klein, P., 1998, "Numerical Simulation of Crack Growth in an Isotropic Solid With Randomized Internal Cohesive Bonds," J. Mech. Phys. Solids, **46**(2), pp. 187–218.
[37] Volokh, K., and Gao, H., 2005, "On the Modified Virtual Internal Bond Method," J. Appl. Mech., **72**(6), pp. 969–971.
[38] Volokh, K., 2007, "Hyperelasticity With Softening for Modeling Materials Failure," J. Mech. Phys. Solids, **55**(10), pp. 2237–2264.
[39] Volokh, K., 2010, "On Modeling Failure of Rubber-Like Materials," Mech. Res. Commun., **37**(8), pp. 684–689.
[40] Trapper, P., and Volokh, K., 2010, "Elasticity With Energy Limiters for Modeling Dynamic Failure Propagation," Int. J. Solids Struct., **47**(25–26), pp. 3389–3396.
[41] Li, J., Mayau, D., and Song, F., 2007, "A Constitutive Model for Cavitation and Cavity Growth in Rubber-Like Materials Under Arbitrary Tri-Axial Loading," Int. J. Solids Struct., **44**(18–19), pp. 6080–6100.
[42] Li, J., Mayau, D., and Lagarrigue, V., 2008, "A Constitutive Model Dealing With Damage Due to Cavity Growth and the Mullins Effect in Rubber-Like Materials Under Triaxial Loading," J. Mech. Phys. Solids, **56**(3), pp. 953–973.
[43] Dal, H., and Kaliske, M., 2009, "A Micro-Continuum-Mechanical Material Model for Failure of Rubber-Like Materials: Application to Ageing-Induced Fracturing," J. Mech. Phys. Solids, **57**(8), pp. 1340–1356.
[44] Talamini, B., Mao, Y., and Anand, L., 2018, "Progressive Damage and Rupture in Polymers," J. Mech. Phys. Solids, **111**, pp. 434–457.
[45] Kumar, A., Francfort, G. A., and Lopez-Pamies, O., 2018, "Fracture and Healing of Elastomers: A Phase-Transition Theory and Numerical Implementation," J. Mech. Phys. Solids, **112**, pp. 523–551.
[46] Lopez-Pamies, O., Idiart, M. I., and Nakamura, T., 2011, "Cavitation in Elastomeric Solids: I–A Defect-Growth Theory," J. Mech. Phys. Solids, **59**(8), pp. 1464–1487.
[47] Pourmodheji, R., Qu, S., and Yu, H., 2016, "The Failure Mechanism for Small Defect in Soft Solids," Proceedings of 53rd Annual Technical Meeting, University of Maryland, Society of Engineering and Science, College Park, MD, Oct. 2–5.
[48] Pourmodheji, R., Qu, S., and Yu, H., 2018, "Two Possible Defect Growth Modes in Soft Solids," J. Appl. Mech., **85**(3), p. 031001.
[49] Mao, Y., Talamini, B., and Anand, L., 2017, "Rupture of Polymers by Chain Scission," Extreme Mech. Lett., **13**, pp. 17–24.
[50] Mao, Y., and Anand, L., 2018, "Fracture of Elastomeric Materials by Crosslink Failure," J. Appl. Mech., **85**(8), p. 081008.
[51] Irwin, G. R., 1948, "Fracture Dynamics," Proceedings of the ASM Symposium on Fracturing of Metals, American Society for Metals, **40**(A), pp. 147–166.
[52] Gao, H., Ji, B., Jäger, I. L., Arzt, E., and Fratzl, P., 2003, "Materials Become Insensitive to Flaws at Nanoscale: Lessons From Nature," Proc. Natl. Acad. Sci., **100**(10), pp. 5597–5600.
[53] Chen, C., Wang, Z., and Suo, Z., 2017, "Flaw Sensitivity of Highly Stretchable Materials," Extreme Mech. Lett., **10**, pp. 50–57.
[54] Volokh, K., 2013, "Review of the Energy Limiters Approach to Modeling Failure of Rubber," Rubber Chem. Technol., **86**(3), pp. 470–487.
[55] Poulain, X., Lopez-Pamies, O., and Ravi-Chandar, K., 2018, "Damage in Elastomers: Healing of Internally Nucleated Cavities and Micro-Cracks," Soft Matter, **14**(22), pp. 4633–4640.
[56] Goriely, A., and Amar, M. B., 2005, "Differential Growth and Instability in Elastic Shells," Phys. Rev. Lett., **94**(19), p. 198103.
[57] Wu, G., Xia, Y., and Yang, S., 2014, "Buckling, Symmetry Breaking, and Cavitation in Periodically Micro-Structured Hydrogel Membranes," Soft Matter, **10**(9), pp. 1392–1399.
[58] Zimberlin, J. A., McManus, J. J., and Crosby, A. J., 2010, "Cavitation Rheology of the Vitreous: Mechanical Properties of Biological Tissue," Soft Matter, **6**(15), pp. 3632–3635.
[59] Jansen, S., Lamy, J.-B., Burlett, R., Cochard, H., Gasson, P., and Delzon, S., 2012, "Plasmodesmatal Pores in the Torus of Bordered Pit Membranes Affect Cavitation Resistance of Conifer Xylem," Plant Cell Environ., **35**(6), pp. 1109–1120.
[60] Joyce, E. M., Moore, J. J., and Sacks, M. S., 2009, "Biomechanics of the Fetal Membrane Prior to Mechanical Failure: Review and Implications," Eur. J. Obs. Gynecol. Reprod. Biol., **144**, pp. S121–S127.
[61] Suo, Z., Zhao, X., and Greene, W. H., 2008, "A Nonlinear Field Theory of Deformable Dielectrics," J. Mech. Phys. Solids, **56**(2), pp. 467–486.
[62] Koh, S. J. A., Li, T., Zhou, J., Zhao, X., Hong, W., Zhu, J., and Suo, Z., 2011, "Mechanisms of Large Actuation Strain in Dielectric Elastomers," J. Polym. Sci. B Polym. Phys., **49**(7), pp. 504–515.
[63] He, T., Zhao, X., and Suo, Z., 2009, "Dielectric Elastomer Membranes Undergoing Inhomogeneous Deformation," J. Appl. Phys., **106**(8), p. 083522.
[64] Plante, J.-S., and Dubowsky, S., 2006, "Large-Scale Failure Modes of Dielectric Elastomer Actuators," Int. J. Solids Struct., **43**(25), pp. 7727–7751.
[65] Zhu, J., Kollosche, M., Lu, T., Kofod, G., and Suo, Z., 2012, "Two Types of Transitions to Wrinkles in Dielectric Elastomers," Soft Matter, **8**(34), pp. 8840–8846.
[66] Hamdi, A., Abdelaziz, M. N., Hocine, N. A., Heuillet, P., and Benseddiq, N., 2006, "A Fracture Criterion of Rubber-Like Materials Under Plane Stress Conditions," Polym. Testing, **25**(8), pp. 994–1005.
[67] Haughton, D.M., 2001, *Elastic Membranes*, London Mathematical Society Lecture Note Series, pp. 233–267.
[68] Dormand, J. R., and Prince, P. J., 1980, "A Family of Embedded Runge-Kutta Formulae," J. Comput. Appl. Math., **6**(1), pp. 19–26.
[69] Mooney, M., 1940, "A Theory of Large Elastic Deformation," J. Appl. Phys., **11**(9), pp. 582–592.
[70] Gent, A., and Thomas, A., 1958, "Forms for the Stored (Strain) Energy Function for Vulcanized Rubber," J. Polym. Sci., **28**(118), pp. 625–628.
[71] Arruda, E. M., and Boyce, M. C., 1993, "A Three-Dimensional Constitutive Model for the Large Stretch Behavior of Rubber Elastic Materials," J. Mech. Phys. Solids, **41**(2), pp. 389–412.
[72] Yeoh, O., 1993, "Some Forms of the Strain Energy Function for Rubber," Rubber Chem. Technol., **66**(5), pp. 754–771.
[73] Ogden, R. W., 1972, "Large Deformation Isotropic Elasticity–On the Correlation of Theory and Experiment for Incompressible Rubberlike Solids," Proc. Roy. Soc. Lond. Math. Phys. Sci., **326**, pp. 565–584.
[74] Yeoh, O., 2002, "Relation Between Crack Surface Displacements and Strain Energy Release Rate in Thin Rubber Sheets," Mech. Mater., **34**(8), pp. 459–474.